Revista de CIENCIAS AGRÍCOLAS

e-ISSN Online 2256-2273

Received: March 11 2026 Accepted: October 28 2026 Published: November 12 2026

Research article: Soil, Plant Nutrition and Water Management

Soil vulnerability to water erosion under intrinsic and rainfall controls

Vulnerabilidad del suelo a la erosión hídrica bajo controles intrínsecos y de precipitación

Clever Gustavo Becerra-Romero [1], Alejandro Becerra-Romero [2], María del Mar Carreño-Sánchez [3], Jhony Armando Benavides-Bolaños [4], Andrés Fernando Echeverri-Sánchez [4]

[1] Corporación Autónoma Regional del Valle del Cauca, Cali, Colombia, clever-gustavo.becerra@cvc.gov.co
[2] Independent Researcher, Medellín, Colombia, alejobero@gmail.com
[3] Universidade Federal de Viçosa, Viçosa, Brazil, maria.sanchez@ufv.br
[4] EIDENAR, Universidad del Valle, Cali, Colombia jhony.benavides@correounivalle.edu.co (Correspondence); andres.echeverri@correounivalle.edu.co

Cite: Becerra-Romero, C. G., Becerra-Romero, A., Carreño-Sánchez, M. M., Benavides-Bolaños, J. A., Echeverri-Sánchez, A. F. (2026). Soil vulnerability to water erosion under intrinsic and rainfall controls. *Revista de Ciencias Agrícolas*, *43*(3), e3313. https://doi.org/10.22267/rcia.2026433.313

ABSTRACT

Water erosion threatens soil conservation in tropical mountain watersheds, where available cartography can help identify areas needing further assessment. This study developed a geographic information systems-based Soil Vulnerability to Water Erosion Index (SVWEI) for the Dagua River watershed, Colombia. Normalized soil erodibility and topographic factors were combined into an intrinsic component, which was then integrated with a rainfall forcing proxy derived from precipitation. Alternative weighting configurations were evaluated for their correspondence with mapped erosion degrees. The selected configuration assigned weights of 0.7 and 0.3 to erodibility and topography, respectively, and 0.8 and 0.2 to the intrinsic component and rainfall forcing. Under baseline conditions, Low and Moderate vulnerability occupied 57.25% and 41.82% of the analyzed area. Moderate vulnerability ranged from 39.77% in the dry perturbation scenario to 44.40% in the wet scenario. Within mapped erosion degrees 3 and 4, 53.69% and 78.44% of the classified area fell into Moderate–High vulnerability. Because the erosion map also informed scenario selection, these associations did not constitute independent validation. The SVWEI provided a relative screening framework for directing field verification and conservation assessment, rather than estimating soil-loss rates, sediment volumes, or event-specific hazards.

Keywords: decision support systems; geographic information systems; land-use planning; multicriteria analysis; Revised Universal Soil Loss Equation; watershed management

RESUMEN

La erosión hídrica amenaza la conservación del suelo en cuencas tropicales de montaña, donde la cartografía disponible puede apoyar la identificación de áreas que requieren una evaluación más detallada. Este estudio desarrolló un Índice de Vulnerabilidad del Suelo a la Erosión Hídrica (IVSEH) basado en sistemas de información geográfica para la cuenca del río Dagua, Colombia. Se combinaron la erodabilidad del suelo y los factores topográficos normalizados en un componente intrínseco, el cual se integró posteriormente con un indicador de forzamiento pluvial derivado de la precipitación. Se examinaron configuraciones alternativas de ponderación mediante su correspondencia descriptiva con los grados de erosión cartografiados. La configuración seleccionada asignó pesos de 0,7 y 0,3 a la erodabilidad y la topografía, respectivamente, y de 0,8 y 0,2 al componente intrínseco y al forzamiento pluvial. Bajo condiciones de línea base, la vulnerabilidad Baja y Moderada ocuparon el 57,25 % y el 41,82 % del área analizada, respectivamente. La vulnerabilidad Moderada varió entre el 39,77 %, en

el escenario de perturbación seca, y el 44,40 %, en el escenario húmedo. Dentro de los grados de erosión cartografiados 3 y 4, respectivamente, el 53,69 % y el 78,44 % del área clasificada se ubicaron en la categoría de vulnerabilidad Moderada–Alta. Dado que el mapa de erosión también fundamentó la selección de los escenarios, estas asociaciones no constituyeron una validación independiente. El IVSEH proporcionó un marco relativo de tamizaje para orientar la verificación en campo y la evaluación de la conservación, en lugar de estimar tasas de pérdida de suelo, volúmenes de sedimentos o riesgos asociados a eventos específicos.

Palabras clave: análisis multicriterio; gestión de cuencas hidrográficas; planificación del uso del suelo; Ecuación Universal Revisada de Pérdida de Suelo; sistemas de apoyo a la toma de decisiones; sistemas de información geográfica

INTRODUCTION

Water erosion threatens soil productivity, water quality, and ecosystem services in tropical mountain watersheds, where erodible soils, steep terrain, rainfall, and land-use pressures interact (Alewell *et al.*, 2019; Borrelli *et al.*, 2020). In steep Andean agricultural watersheds, the co-occurrence of erodible soils, high-intensity rainfall, and land-use pressures accelerates topsoil and soil organic matter (SOM) loss and reduces soil water storage capacity. This, in turn, reduces agricultural productivity, increases sediment delivery to rivers, and elevates risks to water supply infrastructure (Barakat *et al.*, 2023; Mohammed *et al.*, 2025; Rengifo-Rengifo *et al.*, 2022). These impacts span multiple ecosystems and challenge integrated water resources management and territorial planning (Echeverri-Sánchez *et al.*, 2025; Guzman *et al.*, 2019; Terán-Gómez *et al.*, 2025).

Intrinsic vulnerability integrates edaphic susceptibility with geomorphological controls. Specifically, these controls include slope and the potential energy available for overland flow, both of which affect the watershed's predisposition to degradation under variable precipitation conditions (Carvalho *et al.*, 2023; El Moutkine *et al.*, 2024; La Licata *et al.*, 2025; Roy et al., 2020).

The Universal Soil Loss Equation (USLE) and its Revised Universal Soil Loss Equation (RUSLE) provide a widely adopted methodology for estimating soil erosion using rainfall erosivity (R), soil erodibility (K), topography (LS), cover management (C), and support practices (P) (Singh et al., 2023). Geographic information system (GIS) applications have operationalized these factors to map soil loss and erosion at scales ranging from fields to continents, often under data constraints that require coarse climate inputs and generalized soil information (Gutierrez et al., 2023; Nazuhan et al., 2018). Many implementations use these factors as components of a single predictive model, but they do not classify vulnerability using local erosion-degree data derived from high-resolution datasets. This reduces interpretability and limits the practical utility of the resulting maps.

Recent work in erosion mapping increasingly supports a two-step approach: first, delineate intrinsic vulnerability using soil and terrain properties; then, evaluate how external pressures, such as rainfall erosivity and land use, influence that predisposition within broader vulnerability assessments (El Moutkine et al., 2024; Roy et al., 2020).

Within the jurisdiction of the Corporación Autónoma Regional del Valle del Cauca (CVC), the local environmental authority, strategic datasets are publicly available to advance from qualitative diagnosis to a spatially explicit evaluation of intrinsic vulnerability to water erosion. These datasets include a semi-detailed soil survey (1:25,000), a high-resolution digital elevation model (DEM), and a map of erosion classes and degrees derived from satellite imagery at a comparable scale.

Parallel advances in the scientific literature provide mathematical models to quantify soil erodibility and rainfall erosivity under regional conditions, as well as GIS procedures to calculate the LS factor (Desmet & Govers, 1996; Mallick *et al.*, 2016; Olaniya *et al.*, 2020). These resources have not been fully integrated into a single, reproducible methodology that distinguishes intrinsic vulnerability variables (soil erodibility and topographic controls) from extrinsic pressure variables (rainfall erosivity) and uses the existing erosion-degree map as an input for calibration and validation.

This study developed and applied the GIS-based Soil Vulnerability to Water Erosion Index (SVWEI) in the Dagua River watershed, Colombia. The objectives were to separate intrinsic soil–terrain predisposition from precipitation-driven forcing, evaluate alternative weighting configurations by comparing them with mapped erosion degrees, and identify areas for further assessment. It was hypothesized that altering the relative weights of soil, terrain, and rainfall components would change vulnerability classifications, and that wetter perturbation scenarios would increase the representation of higher classes. The intended application was to support CVC and municipal planning teams in prioritizing field verification and conservation assessment, rather than replacing site-specific investigations.

MATERIALS AND METHODS

Study area

The study area is the Dagua River watershed (DRW) in the department of Valle del Cauca, southwestern Colombia. The area covers approximately 109,070 ha and includes the municipalities of Dagua, La Cumbre, Restrepo, Vijes, Yotoco, Calima–El Darién, and Yumbo, as well as a marginal portion of the city of Santiago de Cali. Dagua accounts for 58,585.9 ha (53.7% of the watershed), followed by La Cumbre (22,256.0 ha; 20.4%) and Restrepo (19,000.0 ha; 17.4%), which together account for more than 90% of the watershed. This tropical Andean agricultural watershed features a pronounced topographic gradient from valley bottoms to steep mountain slopes, with land uses ranging from urban and rural settlements to clean-cultivated fields, managed pastures, and forest cover for conservation (Figure 1).

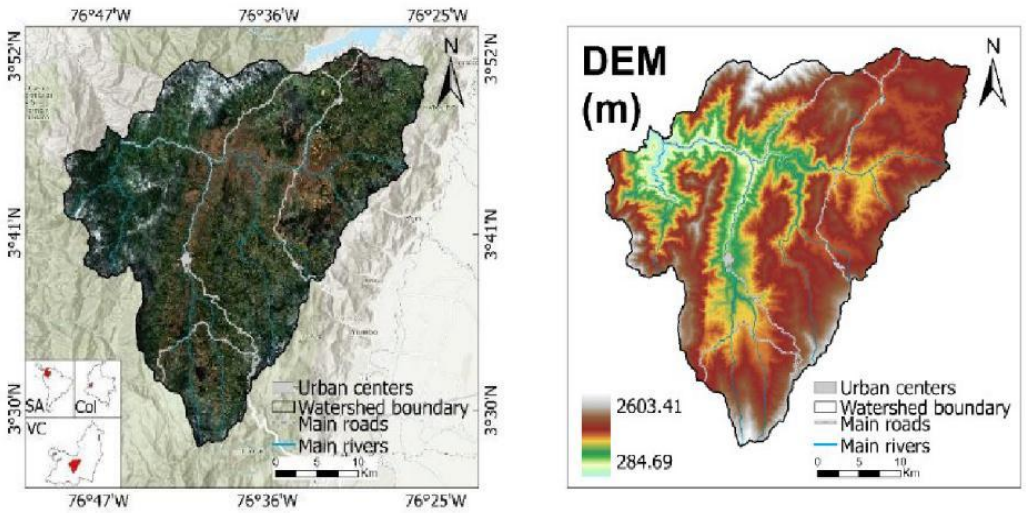

Note. left: true color satellite scene (SA: South America; Col: Colombia; VC: Valle del Cauca); right: Digital Elevation Model (DEM).

Figure 1. *Study area*

Conceptual framework

The SVWEI was structured with two components: an intrinsic vulnerability index that integrated soil erodibility and topography, and a conditioned vulnerability index that modulated this intrinsic predisposition with rainfall erosivity R.

The intrinsic vulnerability Vint was expressed as a weighted linear combination of the minimum-maximum normalized erodibility factor K* and the normalized topographic factor LS* (Equation 1):

$$V_{int}=w_K K^{*}+w_{LS} LS^{*} \qquad \text{(Equation 1)}$$

The weights satisfied $w_K+w_{LS}=1$. Three prescribed configurations were examined: S1, $(w_K,w_{LS})=(0.5,0.5)$; S2, (0.6, 0.4); and S3, (0.7,0.3). These configurations explored alternative emphases on soil and terrain; the weights were not independently estimated measures of physical factor importance.

The full SVWEI combined the normalized intrinsic index V_{int}* with the normalized rainfall erosivity R* (Equation 2):

$$SVWEI=w_V V_{int}^{*}+w_R R^{*} \qquad \text{(Equation 2)}$$

With $w_V+_{wR}=1$, which allowed scenario analysis of the relative influence of intrinsic predisposition and extrinsic forcing. Land cover and management were considered in post-processing by intersecting SVWEI classes with land-cover maps rather than through an explicit multiplicative C factor.

Data sources and preprocessing

Soil erodibility K, topography LS, and rainfall erosivity R were derived from public local cartography and publicly available climate datasets (CVC, 2026; CVC & IGAC, 2025; IGAC & CVC, 2014). Precipitation inputs comprised existing CVC monthly and annual climatological raster layers for 1985–2020, a 36-year reference period. Station records were not assembled or averaged directly in this study. The number of contributing stations and station-specific completeness were unavailable in the accompanying information.

Each raster was minimum–maximum normalized to the interval (0–1) using Equation 3 to ensure comparability among factors:

$$X_{norm}=\frac{X-X_{min}}{X_{max}-X_{min}} \qquad \text{(Equation 3)}$$

Where X corresponded to the factor values in each cell or pixel, and X_{min} and X_{max} were the minimum and maximum values within the watershed. All raster files were projected to a common coordinate system (EPSG: 3115), resampled to 25 m resolution, and clipped to the DRW boundary before index computation.

Soil erodibility (K). Soil erodibility K was estimated using two formulations selected according to the availability of textural and soil organic carbon (SOC) data. Textural fractions (sand, silt, clay) and SOC content were derived from the 1:25,000 semi-detailed local soil survey (CVC & IGAC, 2025). Where granulometric data were missing, representative percentages were inferred from the mapped textural class using USDA's textural triangle. Representative sand/silt/clay percentages were assigned as follows: clay, 20/15/65; silty clay, 5/50/45; loam, 40/40/20; silty clay loam, 10/55/35; clay loam, 32/35/33; sandy loam, 60/25/15; and silt loam, 20/65/15. These assignments approximated mapped classes and did not recover within-class variability. Where SOC

was required, it was estimated from SOM using Equation 4:

$$SOC=SOM/1.724 \quad \text{(Equation 4)}$$

The first formulation (K_1) followed the classical approach of Wischmeier and Smith (1978). Equation 5 defined its texture-size descriptor, and Equation 6 reproduced the documented computational expression. The geometric mean particle diameter DG was first computed using Equation 5:

$$D_G=-3.5f_{clay}-2.0f_{silt}-0.5f_{sand} \quad \text{(Equation 5)}$$

and soil erodibility K_1 was then estimated using Equation 6:

$$K_1=0.0293\left(0.65-D_G+0.24D_G^2\right)\exp\left[-0.0021\left(\frac{OM}{f_{clay}}\right)-0.00037\left(\frac{OM}{f_{clay}}\right)^2-4.02f_{clay}+1.72f_{clay}^2\right]$$

(Equation 6)

where OM corresponded to SOM (%), and $f_{sand,}$ f_{silt} f_{clay} were the fractional contents of sand, silt, and clay, respectively.

The second formulation (K_2) followed the approach described by Zhang *et al.* (2019), as shown in Equation 7:

$$K_2=0.1317f_{csand}f_{clay\text{-}silt}f_{soc}f_{hisand} \quad \text{(Equation 7)}$$

where f_{csand} accounted for coarse sand, $f_{clay\text{-}silt}$ represented the clay-silt ration, fsoc captured SOC effects, and f_{hisand} adjusted for high sand content, each expressed as non-linear functions of sand (ms), silt (m_{silt}), clay (m_{clay}), and SOC, as shown in Equations 8, 9, 10, and 11:

$$f_{csand}=0.2+0.3^{\left(-0.256m_s\left(1-\frac{m_{silt}}{100}\right)\right)} \quad \text{(Equation 8)}$$

$$f_{clay\text{-}silt}=\left(\frac{m_{silt}}{m_{clay}+m_{silt}}\right)^{0.3} \quad \text{(Equation 9)}$$

$$f_{soc}=1-\frac{0.25SOC}{SOC+e^{3.72-2.95SOC}} \quad \text{(Equation 10)}$$

$$f_{hisand}=1-\frac{0.7\left(1-\frac{m_s}{100}\right)}{\left(1-\frac{m_s}{100}\right)+e^{\left(-5.51+22.9\left(1-\frac{m_s}{100}\right)\right)}} \quad \text{(Equation 11)}$$

Both K_1 and K_2 were rasterized to 25 m resolution and normalized to obtain K_1* and K_2* (Figure 2).

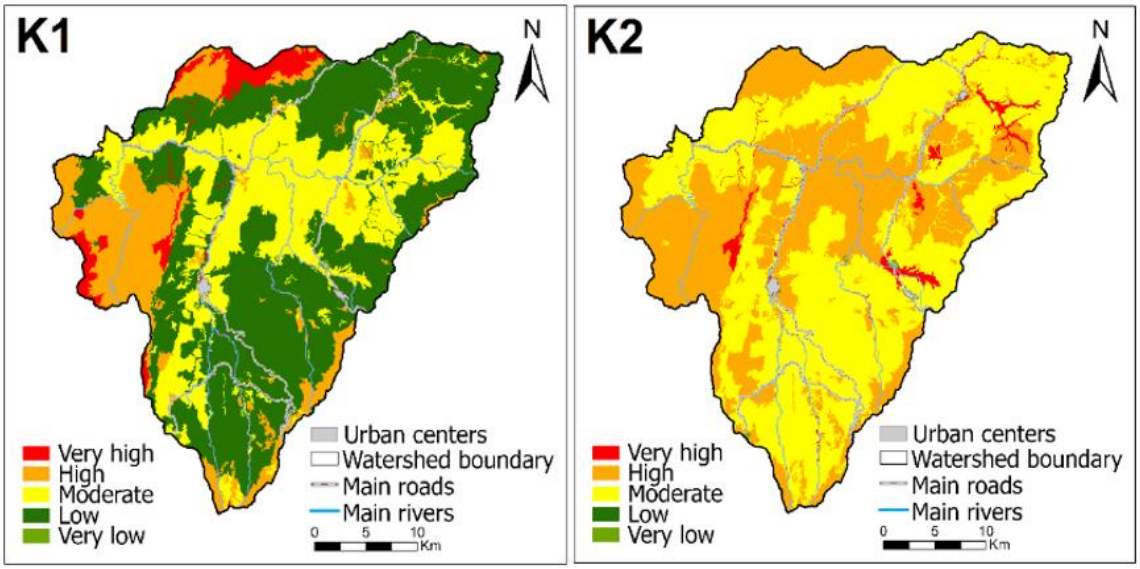

Note. Left: K_1* calculated following Wischmeier and Smith (1978); right: K_2* calculated following Zhang *et al.* (2019). Both were normalized to a 0–1 scale and classified into five vulnerability classes.

Figure 2. *Normalized erodibility classes for the implemented K_1 and K_2 formulations. Colors indicate relative classes, not measured soil-loss rates*

Topographic factor (LS). The topographic component was estimated using a simplified GIS implementation within the RUSLE framework (Desmet & Govers, 1996). A 5 m DEM was depression-filled and resampled to 25 m using bilinear interpolation. GIS flow-routing methods provide alternative representations of drainage pathways (Holmgren, 1994; Tarboton, 1997). This study used D8 to derive flow direction and accumulation. Slope was calculated in degrees with a Z-factor of 1. An accumulation-based length surrogate, λ=(F+1)×25, where F was the number of contributing cells, was used to calculate L=(λ⁄22.13)^m. The exponent m was 0.2, 0.3, 0.4, or 0.5 for slopes below 1°, 1–<3°, 3–<5°, or ≥5°, respectively. The implemented steepness expression used a 9° breakpoint, and LS=L × S.

Rainfall erosivity factor (R) and climatic scenarios. The R factor was computed from monthly and annual precipitation data using two empirical formulations commonly applied when high-frequency intensity data are unavailable.

One erosivity formulation (Rutebuka *et al.*, 2020) related R to the Modified Fournier Index (MFI) as described in Equation 12:

$$R=256MFI^{1.065} \qquad \text{(Equation 12)}$$

where MFI was calculated using Equation 13:

$$MFI=\sum_{i=1}^{12}\frac{P_i^2}{P_a} \qquad \text{(Equation 13)}$$

where P_i and P_a represented the monthly and annual precipitation climatologies, respectively, for the 1985–2020 reference period.

The operational rainfall layer was generated using the monthly precipitation expression shown in Equation 14. It was interpreted as an uncalibrated rainfall forcing proxy rather than an independently validated estimate of physical erosivity.

$$R=\sum_{i=1}^{12} 1.735\times10^{\left(1.5\log_{10}\left(\frac{p_i^2}{P_a}\right)-0.08188\right)} \quad \text{(Equation 14)}$$

Only the normalized rainfall proxy entered the SVWEI; physical erosivity units were not assigned to the operational proxy without verification of its formulation and calibration.

The formulation of Arnoldus (1980) was retained to generate the operational baseline R layer and the derived R_{max} and R_{min} used in all SVWEI integrations given its broader application for R estimation within the RUSLE framework. Equation 14 defines the operational rainfall proxy used in the reported index configurations.

To analyze sensitivity to climate variability, two contrasting erosivity scenarios were generated. For each pixel, the maximum mean monthly precipitation was identified, and months with $P_{month} \geq 0.8_{Pmax\ month}$ were flagged as relatively wet; corresponding areas were up-weighted by 1.2 to obtain a wet scenario R_{max}, while the rest of the areas were down-weighted by 0.8 to simulate a drier scenario Rmin. All R layers were normalized to (0–1) prior to integration into the index.

Rainfall perturbations were used to examine classification sensitivity, that is, for each pixel. Months with $Pi \geq 0.8_{Pmax}$ where Pmax was the largest monthly precipitation mean, were identified as relatively wet. Precipitation in these flagged months was multiplied by 1.2 or 0.8 for the wet and dry perturbations, respectively, and unflagged months were unchanged. The multipliers represented exploratory ±20% changes, not estimated return periods, observed extremes, or climate projections. The scenario comparison was exploratory; annual aggregation and normalization references require explicit verification before the reported class differences can be interpreted as calibrated rainfall responses.

Vulnerability Modeling

Intrinsic vulnerability scenarios. The two erodibility formulations were initially compared. The normalized K_2 layer was retained for the subsequent intrinsic weighting exercise, which examined S1–S3. S3 was selected for integration with rainfall forcing based on descriptive correspondence with mapped erosion degrees. This comparison supported configuration selection rather than independent validation.

Full SVWEI scenarios and classification. The full index combined V_{int}* and R* under four prescribed configurations: W1, (w_v,w_R)=(0.5,0.5); W2, (0.6, 0.4); W3, (0.7, 0.3); and W4, (0.8, 0.2). W4 was retained for the reported baseline and rainfall perturbation comparisons.

Both V_{int} and SVWEI were classified into five qualitative vulnerability levels based on percentage thresholds: Very low: SVWEI < 20%; Low: 20% ≤ SVWEI < 40%; Moderate: 40% ≤ SVWEI <60%; High: 60% ≤ SVWEI < 80%; Very high: SVWEI ≥ 80%.

Fixed intervals of 0.2 were applied across W1–W4 as operational categories for comparing vulnerability configurations (Figure 3). These thresholds were not calibrated physical erosion thresholds or probabilities of degradation. W4 (w_{Vint}=0.8, w_R=0.2) was retained following descriptive comparison with mapped erosion degrees; this selection did not constitute independent validation.

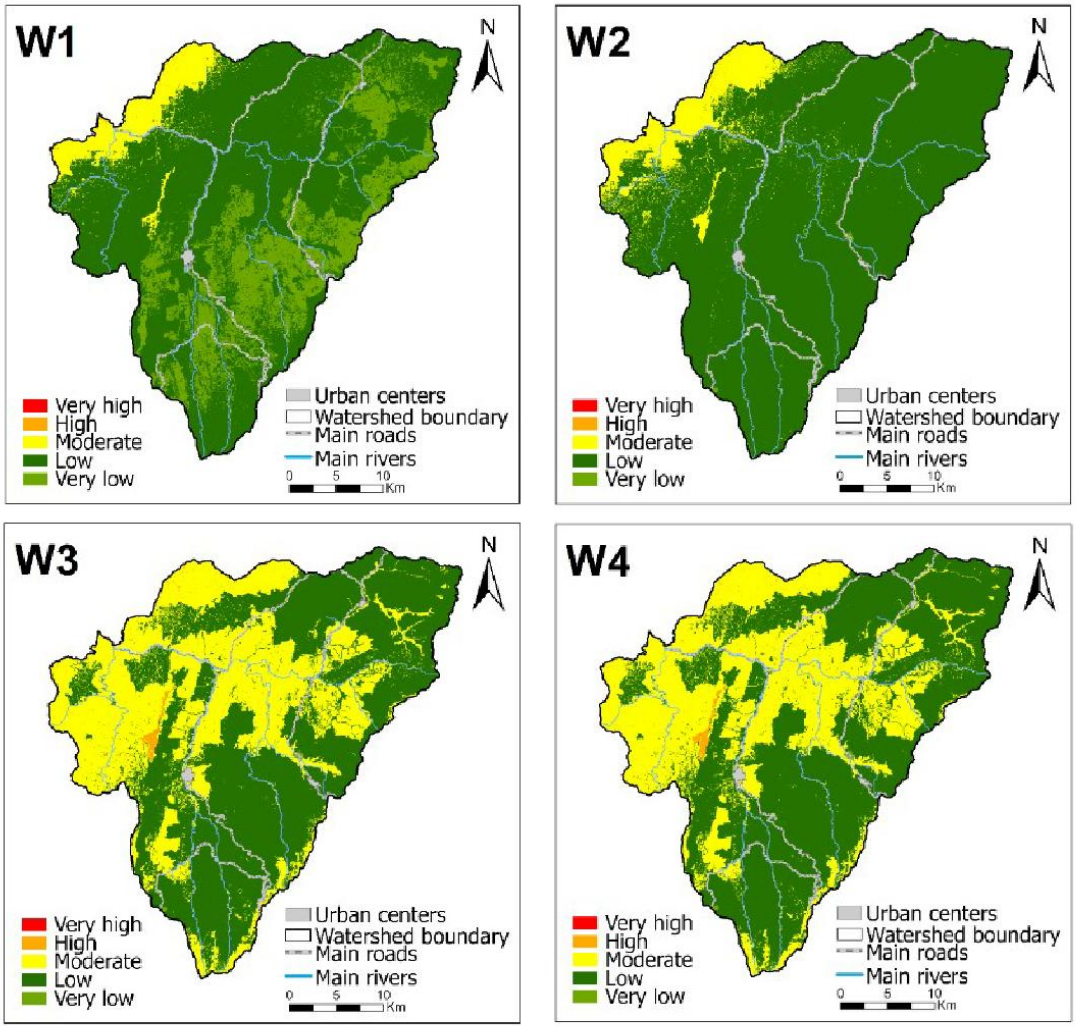

Figure 3. *Baseline SVWEI under W1–W4. Intrinsic/rainfall weights were 0.5/0.5, 0.6/0.4, 0.7/0.3, and 0.8/0.2, respectively*

Cartographic Comparison and Spatial Analysis

Comparison with mapped erosion degrees. The SVWEI was cross-tabulated against the available 1:50,000 erosion-degree map using Tabulate Area in ArcGIS Pro version 3.6 (ESRI, Redlands, CA, USA). Areas were summarized by vulnerability class and mapped erosion degree. Because this map also informed configuration selection, the comparison was descriptive and did not provide independent validation. Vulnerability classes represented relative predisposition, whereas erosion degrees represented mapped degradation; that is, a one-to-one correspondence between their category labels was not assumed. For each mapped erosion degree j, its Moderate–High share was calculated as described in Equation 15:

$$100(A_{j,\,\text{Moderate}}+A_{j,\,\text{High}})/\sum_c A_{j,c} \qquad \text{(Equation 15)}$$

Where $A_{j,c}$ was the area classified in mapped erosion degree j and SVWEI vulnerability class c, and the denominator summed this area across all vulnerability classes included in Table 3.

RESULTS

Soil erodibility (K). Two formulations were used to estimate K: the first (K_1) based on the work of Wischmeier and Smith (1978), and the second (K_2) based on Zhang *et al*. (2019). Although K_2 produced lower absolute K values than K_1, the normalized K_2 values showed a stronger internal contrast, with a larger share of the watershed classified as Moderate to High vulnerability (Table 1). K_1 concentrated most of the watershed in Low to Moderate classes, indicating a more conservative spatial classification of K.

Table 1. *Distribution of normalized erodibility and topographic classes in the study area*

Vulnerability level	K_1 Area (ha)	K_1 Area (%)	K_2 Area (ha)	K_2 Area (%)	LS Factor Area (ha)	LS Factor Area (%)
Very low	381.88	0.35	381.88	0.35	81,034.75	74.43
Low	54,764.94	50.21	0.00	0.00	24,182.69	22.21
Moderate	31,209.94	28.61	60,598.88	55.56	2,770.13	2.54
High	17,832.19	16.35	45,019.44	41.28	688.75	0.63
Very high	4,879.81	4.47	3,068.56	2.81	193.31	0.18
Total	109,068.80	100.00	109,068.80	100.00	108,869.60	100.00

Note. K_1 was estimated using the formulation of Wischmeier and Smith (1978), and K_2 was estimated using the formulation of Zhang *et al*. (2019).

Topographic factor (LS). The LS classification was skewed toward the lower categories: Very low LS had 81,034.75 ha (74.43%), and Low had 24,182.69 ha (22.21%), leaving 2,770.13 ha (2.54%) and 688.75 ha (0.63%) for the Moderate and the High classes, respectively. Only 193.31 ha (0.18%) was classified in the Very high class. Areas with High and Very high LS classes were concentrated in steep mountainous sectors of the Dagua municipality. The concentration in Very Low and Low normalized LS classes described the distribution of the processed topographic indicator; it did not establish that most of the watershed had gentle terrain or negligible topographic influence.

Intrinsic vulnerability index V_{int}. The initial comparison between erodibility formulations produced different distributions of intrinsic vulnerability. Moderate vulnerability occupied 30.08% of the analyzed area with the K_2 formulation associated with Zhang *et al.* (2019), compared with 11.95% using K_1. These differences showed that the erodibility representation affected the resulting intrinsic classifications. In the subsequent weighting comparison using K_2*, increasing the weight assigned to erodibility altered the distribution of vulnerability classes. S3 (w_K=0.7, w_{LS}=0.3) showed greater representation of mapped erosion degrees 3–4 within Moderate vulnerability than S1. This descriptive correspondence supported retaining S3 as the intrinsic baseline for integration with rainfall forcing.

Rainfall erosivity (R) and climatic scenarios. The normalized rainfall forcing proxy was concentrated in the Very Low and Low classes. The reported wet perturbation increased the area in higher proxy classes, whereas the dry perturbation increased the Very Low share (Table 2). These classes expressed relative positions within the adopted scaling and did not establish physically low rainfall erosivity or quantify storm intensity.

Table 2. *Distribution of normalized rainfall forcing classes under three perturbation conditions*

Vulnerability class	R_{max} Area (ha)	R_{max} Area (%)	R Area (ha)	R Area (%)	R_{min} Area (ha)	R_{min} Area (%)
Very low	92,745.81	84.91	96,986.00	88.76	99,112.13	90.71
Low	8,714.63	7.98	6,926.06	6.34	5,834.31	5.34
Moderate	4,396.56	4.03	4,537.56	4.15	3,818.00	3.49
High	3,073.50	2.81	812.94	0.74	498.88	0.46
Very high	298.13	0.27	0.00	0.00	0.00	0.00
Total	109,228.63	100.00	109,262.56	100.00	109,263.31	100.00

Correspondence between SVWEI classes and erosion degrees. Baseline SVWEI was dominated by Low and Moderate vulnerability, covering 57.25% and 41.82% of the analyzed area, respectively (Table 4). Within mapped erosion degrees 1–4, the proportions occurring in Moderate–High SVWEI were 23.15%, 20.17%, 53.69%, and 78.44%, respectively (Table 3). Thus, degrees 3–4 had greater representation in these vulnerability classes, although the relationship was not strictly monotonic across all erosion degrees. These percentages described cartographic correspondence rather than classification accuracy. Areas coded as URB were concentrated in the Very Low class. NAT, URB, and NA were retained as separate map categories and were not interpreted as numerical erosion degrees.

Table 3. *Area-based correspondence between baseline SVWEI classes and mapped erosion degrees*

Erosion grade	Very Low area (ha)	Very Low (%)	Low area (ha)	Low (%)	Moderate area (ha)	Moderate (%)	High area (ha)	High (%)
1	24.63	6.47	3,763.50	6.04	1,122.69	2.47	18.31	2.90
2	25.06	6.58	34,224.81	54.91	8,616.69	18.92	34.63	5.49
3	26.31	6.91	7,286.50	11.69	8,417.69	18.49	62.00	9.83
4	7.94	2.09	2,367.06	3.80	8,613.06	18.92	25.63	4.06
NAT	20.25	5.32	14,412.25	23.12	18,481.00	40.59	488.50	77.48
URB	276.44	72.63	172.44	0.28	122.31	0.27	0.00	0.00
NA	0.00	0.00	99.19	0.16	158.63	0.35	1.44	0.23
Total	380.63	100.00	62,325.75	100.00	45,532.06	100.00	630.50	100.00

Note. NAT: natural erosion; URB: urban zone; NA: no information available. Percentages in the existing columns were calculated within each SVWEI class; each percentage column totaled 100%. Erosion-degree-specific percentages reported in the text used the total classified area within the corresponding erosion degree. NAT, natural erosion; URB, urban zone; NA, no information.

Moderate vulnerability occupied 39.77%, 41.82%, and 44.40% under dry, baseline, and wet conditions, respectively. High vulnerability occupied 0.50%, 0.58%, and 0.77% (Figure 4; Table 4). The wet–dry differences were 4.63 percentage points for Moderate and 0.27 percentage points for High vulnerability.

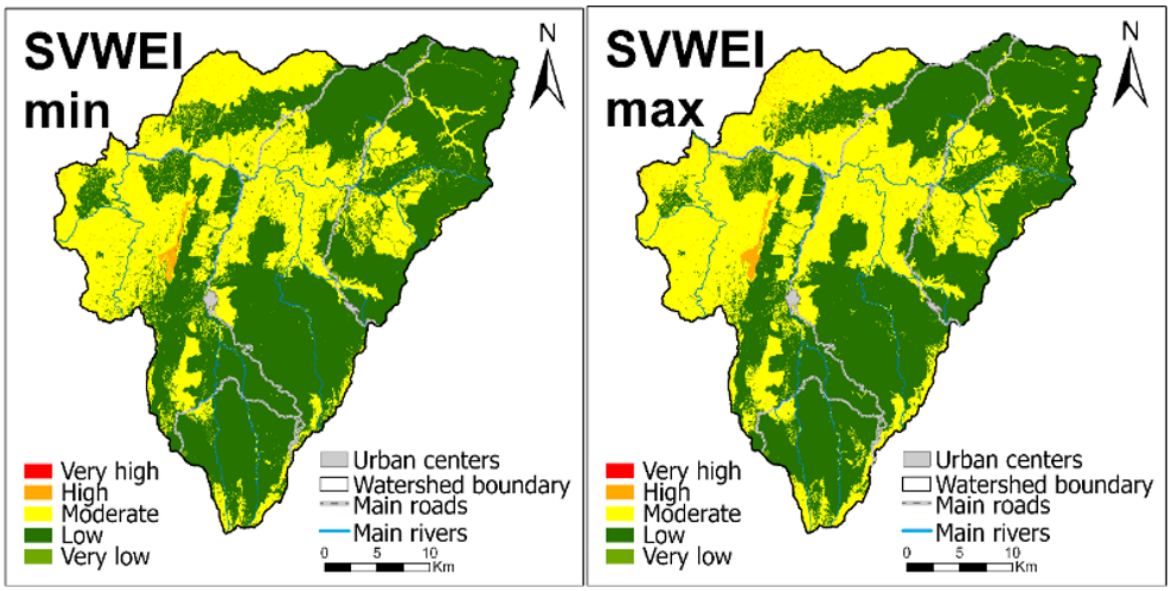

Figure 4. *SVWEI under dry and wet precipitation perturbations using the selected W4 configuration*

Table 4. *Distribution of SVWEI classes under baseline, wet, and dry perturbation conditions*

Vulnerability class	Wet scenario area (ha)	Wet scenario (%)	Baseline area (ha)	Baseline (%)	Dry scenario area (ha)	Dry scenario (%)
Very low	380.63	0.35	380.63	0.35	380.56	0.35
Low	59,310.81	54.48	62,325.75	57.25	64,646.38	59.38
Moderate	48,341.19	44.40	45,532.06	41.82	43,292.44	39.77
High	836.19	0.77	630.50	0.58	549.63	0.50
Very high	0.06	0.00	0.06	0.00	0.19	0.00
Total	108,868.90	100.00	108,869.00	100.00	108,869.20	100.00

A shift in land use composition across SVWEI classes was observed, from predominantly built-up categories at Very Low vulnerability to conservation and agricultural covers at Low–Moderate vulnerability, and ultimately to sustainable-use areas dominating the High and entirely defining the Very High class.

DISCUSSION

Intrinsic controls versus topography

The contrasting K classifications indicated that the representation of erodibility influenced the spatial pattern inherited by the intrinsic index. Differences among estimation methods have also been documented at the hillslope scale, supporting caution when interpreting alternative K formulations as equivalent representations of soil susceptibility (Kruk, 2020). Relationships among K, texture, and other soil properties vary across environments, while global comparisons show that algorithm selection can affect mapped erodibility patterns (Huang *et al.*, 2022; Yang *et al.*, 2024). In the DRW, 96.64% of the normalized LS layer fell into the Very Low and Low classes. Together with the selected weighting, this distribution favored a stronger expression of K in

the composite index. However, the concentration in low normalized LS classes did not indicate predominantly gentle terrain or demonstrate the physical dominance of soil properties over topography.

Sensitivity to K representation and K–LS interaction

Changing the erodibility representation and its assigned weight altered the intrinsic classifications, affecting the identification of areas requiring further assessment. This sensitivity was consistent with evidence that K estimates depend on both soil characteristics and the selected algorithm (Huang *et al.*, 2022; Yang *et al.*, 2024). The selected S3 configuration emphasized erodibility, but its correspondence with mapped erosion degrees did not independently establish the relative contributions of K and LS. Accordingly, moderate-vulnerability areas should remain candidates for verification where agricultural disturbance or discontinuous vegetation could favor runoff and sediment detachment. Experimental evidence that vegetation and slope jointly influence erosion supports considering these conditions together when interpreting screening results (Sun *et al.*, 2021).

Rainfall forcing and classification sensitivity

The rainfall perturbations altered the reported vulnerability distributions, though the Low and Moderate classes remained predominant. These changes offered an exploratory indication of classification sensitivity rather than evidence of observed climatic trends or event-specific responses. The regional bimodal pattern of erosive rainfall supports examining seasonal forcing, although monthly precipitation summaries cannot capture the intensity and energy of individual storms (Calero Mosquera *et al.*, 2021). Comparisons of rainfall estimators also show that their performance depends on temporal information and regional evaluation, limiting direct interpretation of an uncalibrated proxy as physical erosivity (Ma & Zheng, 2022; Cardoso *et al.*, 2022). The relatively limited influence of rainfall on the SVWEI also reflected its W4 weight of 0.2 and the normalized proxy distribution. It should not be interpreted as evidence that rainfall was physically unimportant within the watershed.

Cartographic correspondence and screening value

Areas mapped as erosion degrees 3–4 were more prevalent in Moderate–High SVWEI than degrees 1–2, supporting further evaluation of the index for prioritization. Similar GIS-based assessments have used spatial erosion indicators to identify areas requiring conservation attention (Debebe *et al.*, 2025; Santos *et al.*, 2025). Nevertheless, because the same erosion map informed configuration selection, the observed correspondence did not constitute independent validation. Differences could also reflect spatial support and processing choices: LS estimates depend on DEM source and resolution, while changes in terrain detail affect the identification of hydrological pathways and sensitive areas (Lu *et al.*, 2020; Thomas *et al.*, 2016, Thomas *et al.*, 2017). Resampling to 25 m did not eliminate the uncertainty associated with the 1:50,000 reference map. Consequently, the comparison supported directing further assessment rather than diagnosing current erosion severity.

Land cover and management implications

The land-cover intersection indicated that some higher-vulnerability areas retained natural or semi-natural vegetation. Because cover was considered after index construction, these classifications reflected underlying predisposition rather than measured erosion beneath vegetation. Evidence from forest conversion and simulated-rainfall studies supports maintaining protective cover in such settings, although the magnitude of its effect was not measured in the DRW (Chu *et al*., 2026; Niu *et al*., 2025).

Experimental findings also show that vegetation protection depends on slope and rainfall conditions, while agricultural assessments emphasize the combined influence of terrain and management (Sun *et al*., 2021; Sodoke *et al*., 2025). These findings supported targeted verification in vegetated higher-vulnerability areas and assessment of cover continuity and runoff pathways in cultivated sectors. Where appropriate, vegetated buffers could complement other conservation practices by intercepting incoming loads, with effectiveness depending on their design and loading conditions (Jiang *et al*., 2020). The baseline Very High class occupied only 0.06 ha, making its land-cover composition unsuitable for watershed-wide inference.

Limitations and future evaluation

Inferred texture fractions introduced uncertainty because K estimates depend on soil-property representation and algorithm choice (Huang *et al.*, 2022; Yang *et al.*, 2024). Monthly precipitation inputs could not capture short-duration intensity or event energy, and the rainfall proxy lacked independent regional calibration (Ma & Zheng, 2022). Consequently, localized storm-driven erosion could differ substantially from the mapped screening classes. Rainfall-triggered landslides and debris flows involved additional geotechnical and hydrological controls outside the SVWEI's scope; their assessment required separate hazard methods. Official data provenance did not overcome these temporal limitations. Similarly, DEM source, resolution, and the simplified LS implementation constrained topographic interpretation (Lu *et al.*, 2020). Future work should verify computational expressions and normalization references, evaluate rainfall forcing against sub-hourly observations, and test prioritization using spatially independent erosion observations. These improvements would strengthen the index's use for directing field verification and conservation assessment, while soil-loss rates, sediment volumes, and event-specific hazards remained outside its objectives.

CONCLUSIONS

This study examined vulnerability to water erosion. The SVWEI methodology demonstrated that separating intrinsic watershed fragility from climatic forcing is feasible using available soil, terrain, and rainfall data, and that it can reveal important spatial differences in vulnerability in complex terrains such as the DRW. The SVWEI provided a relative screening framework that separated soil–terrain predisposition from precipitation-derived forcing. Under the selected configuration, Low and Moderate vulnerability occupied 57.25% and 41.82% of the analyzed area, respectively. Moderate vulnerability ranged from 39.77% under the dry perturbation to 44.40% under the wet perturbation. The influence of erodibility on the classifications depended on its representation, normalization, and assigned weight. Correspondence with mapped erosion degrees supported further evaluation of the screening approach but did not constitute independent validation. The index identified candidate areas for field verification and conservation assessment; it did not estimate soil-loss rates, sediment volumes, or event-specific hazards. Verification of computational details and evaluation against independent observations remained necessary before stronger performance claims could be made. Even with the current limitations, the study provides a basis for supporting soil conservation planning and climate-sensitive erosion assessment in data-limited Andean tropical watersheds.

AUTHOR CONTRIBUTIONS

Conceptualization, C.G.B.R. and A.B.R.; Investigation, C.G.B.R. and A.B.R.; Methodology, C.G.B.R. and A.B.R.; Software, M.M.C.S.; Visualization, M.M.C.S.; Data Curation, J.A.B.B.; Formal Analysis, J.A.B.B.; Validation, J.A.B.B.; Writing—Review & Editing, J.A.B.B.; Funding Acquisition, A.F.E.S.; Project Administration, A.F.E.S.; Supervision, A.F.E.S.; Writing—Original Draft Preparation, A.F.E.S.

ACKNOWLEDGMENTS

The authors would like to thank the Corporación Autónoma Regional del Valle del Cauca (CVC) and Universidad del Valle for their institutional support.

FUNDING

This research was funded through Inter-Administrative Contract No. 0792 of 2024 (Project Code 42061F), executed between CVC and Universidad del Valle.

CONFLICT OF INTEREST

The authors declare that there is no conflict of interest.

REFERENCES

Alewell, C., Borrelli, P., Meusburger, K., & Panagos, P. (2019). Using the USLE: Chances, challenges and limitations of soil erosion modelling. *International Soil and Water Conservation Research*, *7*(3), 203-225. https://doi.org/10.1016/j.iswcr.2019.05.004

Arnoldus, H. M. J. (1980). An approximation of the rainfall factor in the universal soil loss equation. In M. De Boodt & D. Gabriel (Eds.), *Assessment of Erosion* (pp. 127–132). John Wiley and Sons.

Barakat, A., Rafai, M., Mosaid, H., Islam, M. S., & Saeed, S. (2023). Mapping of water-induced soil erosion using machine learning models: A case study of Oum Er Rbia Basin (Morocco). *Earth Systems and Environment*, *7*(1), 151–170. https://doi.org/10.1007/s41748-022-00317-x

Borrelli, P., Robinson, D., Panagos, P., Lugato, E., Yang, J., Alewell, C., Wuepper, D., Montanarella, L., & Ballabio, C. (2020). Land use and climate change impacts on global soil erosion by water (2015-2070). *Proceedings of the National Academy of Sciences*, *117*(36), 21994–22001. https://doi.org/10.1073/pnas.2001403117

Calero Mosquera, D., Martínez López, C., & Menjívar Flores, J. C. (2021). Evaluation of models to estimate rainfall erosivity in Valle del Cauca, Colombia. *Acta Agronomica*, *70*(2), 198-210. https://doi.org/10.15446/acag.v70n2.95115

Cardoso, D. P., Avanzi, J. C., Ferreira, D. F., Acuña-Guzman, S. F., Silva, M. L. N., Pires, F. R., & Curi, N. (2022). Rainfall erosivity estimation: Comparison and statistical assessment among methods using data from Southeastern Brazil. *Revista Brasileira de Ciencia Do Solo*, *46,* e0210122. https://doi.org/10.36783/18069657rbcs20210122

Carvalho, M. L., Maciel, V. F., Bordonal, R. de O., Carvalho, J. L. N., Ferreira, T. O., Cerri, E. P., & Cherubin, M. R. (2023). Stabilization of organic matter in soils: drivers, mechanisms, and analytical tools – a literature review. *Revista Brasileira de Ciencia Do Solo*, *47,* e0230130. https://doi.org/10.36783/18069657rbcs20220130

Chu, J., Cao, Y., Shen, Y., Teng, Q., Liao, J., Sun, Y., Zhang, D., Liang, Y., Huang, K., Shi, H., & Xu, G. (2026). Evaluation of forest conversion effects on soil erosion and soil organic carbon using 137Cs and 210Pbex tracers in the low mountain–hill region of Southwest China. *Frontiers in Environmental Science*, *13,* 1703401. https://doi.org/10.3389/fenvs.2025.1703401

Corporación Autónoma Regional del Valle del Cauca - CVC. (2026). GeoCVC Visor geográfico del Valle del Cauca. https://portal-geo.cvc.gov.co/inicio/

Corporación Autónoma Regional del Valle del Cauca - CVC, & Instituto Geográfico Agustín Codazzi - IGAC. (2025). Levantamiento semidetallado de suelos del departamento del Valle del Cauca escala 1:25.000. Ecopedia. https://ecopedia.cvc.gov.co/suelo/caracteristicas-del-suelo/levantamiento-semidetallado-de-suelos-del-departamento-del-valle

Debebe, W., Yirgu, T., & Debele, M. (2025). Assessing soil erosion potential for prioritization of land risk area in the Sala watershed of Ari zone, South Ethiopia. *Frontiers in Environmental Science*, *13,* 1495923. https://doi.org/10.3389/fenvs.2025.1495923

Desmet, P. J. J., & Govers, G. (1996). A GIS procedure for automatically calculating the USLE LS factor on topographically complex landscape units. *Journal of Soil and Water Conservation*, *51*(5), 427–433. https://doi.org/10.1080/00224561.1996.12457102

Echeverri-Sánchez, A. F., Olaya, R. A., Carreño-Sánchez, M. del M., Becerra-Romero, C. G., & Benavides-Bolaños, J. A. (2025). Soil sealing vulnerability in high-value agricultural land: A multicriteria GIS-based approach. *Revista de Ciencias Agrícolas*, *42*(3), e3277. https://doi.org/10.22267/rcia.20254203.277

El Moutkine, K., Tabyaoui, H., El Hammichi, F., El Hassani, F., & Benabdelhadi, M. (2024). Assessing water erosion vulnerability in the lower ziz watershed: Integrating PAP/RAC methodology with remote sensing and GIS. *BIO Web of Conferences*, *115,* 01002. https://doi.org/10.1051/bioconf/202411501002

Gutierrez, L., Huerta, A., Sabino, E., Bourrel, L., Frappart, F., & Lavado-Casimiro, W. (2023). Rainfall erosivity in Peru: A new gridded dataset based on GPM-IMERG and comprehensive assessment (2000–2020). *Remote Sensing*, *15*(22), 5432. https://doi.org/10.3390/rs15225432

Guzman, C. D., Hoyos-Villada, F., Da Silva, M., Zimale, F. A., Chirinda, N., Botero, C., Morales Vargas, A., Rivera, B., Moreno, P., & Steenhuis, T. S. (2019). Variability of soil surface characteristics in a mountainous watershed in Valle del Cauca, Colombia: Implications for runoff, erosion, and conservation. *Journal of Hydrology*, *576*, 273–286. https://doi.org/10.1016/j.jhydrol.2019.06.002

Holmgren, P. (1994). Multiple flow direction algorithms for runoff modelling in grid based elevation models: An empirical evaluation. *Hydrological Processes, 8*(4), 327-334. https://doi.org/10.1002/hyp.3360080405

Huang, X., Lin, L., Ding, S., Tian, Z., Zhu, X., Wu, K., & Zhao, Y. (2022). Characteristics of soil erodibility K value and its influencing factors in the Changyan Watershed, Southwest Hubei, China. *Land*, *11*(1), 134. https://doi.org/10.3390/land11010134

Instituto Geográfico Agustín Codazzi - IGAC, & Corporación Autónoma Regional del Valle del Cauca - CVC. (2014). Levantamiento semidetallado de suelos escala 1:25,000 de las cuencas priorizadas por la Corporación Autónoma Regional del Valle del Cauca – CVC 4888 IGAC-087 CVC DE 2014. https://ecopedia.cvc.gov.co/suelo/caracteristicas-del-suelo/levantamiento-semidetallado-de-suelos-escala-125000-de-las-cuencas

Jiang, F., Preisendanz, H. E., Veith, T. L., Cibin, R., & Drohan, P. J. (2020). Riparian buffer effectiveness as a function of buffer design and input loads. *Journal of Environmental Quality*, *49*(6), 1599–1611. https://doi.org/10.1002/jeq2.20149

Kruk, E. (2020). Use of chosen methods for determination of the USLE soil erodibility factor on the example of loess slope. *Journal of Ecological Engineering*, *22*(1), 151–161. https://doi.org/10.12911/22998993/128861

La Licata, M., Adeniyi, O. D., Ellerbrock, R. H., Bhattarai, N., Bosino, A., Papke, N., Schaller, J., & Maerker, M. (2025). FTIR-derived soil degradation indices and stochastic modelling of organic matter–sediment dynamics in a Mediterranean watershed: A Northern Apennines case study. *PLOS ONE*, *20*(8), e0330252. https://doi.org/10.1371/journal.pone.0330252

Lu, S., Liu, B., Hu, Y., Fu, S., Cao, Q., Shi, Y., & Huang, T. (2020). Soil erosion topographic factor (LS): Accuracy calculated from different data sources. *Catena*, *187,* 104334. https://doi.org/10.1016/j.catena.2019.104334

Ma, X., & Zheng, M. (2022). Statistical evaluation of proxies for estimating the rainfall erosivity factor. *Scientific Reports*, *12*(1), 12092. https://doi.org/10.1038/s41598-022-15271-x

Mallick, J., Al-Wadi, H., Rahman, A., Ahmed, M., & Abad Khan, R. (2016). Spatial variability of soil erodibility and its correlation with soil properties in semi-arid mountainous watershed, Saudi Arabia. *Geocarto International*, *31*(6), 661–681. https://doi.org/10.1080/10106049.2015.1073368

Mohammed, J. A., Gashaw, T., & Yimam, Z. A. (2025). Identification of erosion-prone watersheds for prioritizing soil and water conservation in a changing climate using morphometric analysis and GIS. *Natural Hazards*, *121*(4), 4171–4189. https://doi.org/10.1007/s11069-024-06952-z

Nazuhan, M., Rahaman, Z. A., & Othman, Z. (2018). A review on rainfall erosivity (R factor) in universal soil loss equation. *International Journal of Academic Research in Business and Social Sciences*, *8*(2), 816–822. https://doi.org/10.6007/ijarbss/v8-i2/3988

Niu, L., Hu, J., Li, P., Zhao, G., & Mu, X. (2025). The effect of vegetation restoration on erosion processes and runoff on a hillslope under simulated rainfall. *Water*, *17*(16), 2411. https://doi.org/10.3390/w17162411

Olaniya, M., Bora, P. K., Das, S., & Chanu, P. H. (2020). Soil erodibility indices under different land uses in Ri-Bhoi district of Meghalaya (India). *Scientific Reports*, *10*(1), 14986. https://doi.org/10.1038/s41598-020-72070-y

Rengifo-Rengifo, I.-Y., Muñoz-Gomez, F.-A., & Toro-Trochez, O.-A. (2022). Modelo USLE para estimar la erosión hídrica en siete municipios de la zona andina colombiana. *Biotecnología En El Sector Agropecuario y Agroindustrial*, *20*(2), 29–44. https://doi.org/10.18684/rbsaa.v20.n2.2022.1738

Roy, P., Pal, S. C., Arabameri, A., Chakrabortty, R., Pradhan, B., Chowdhuri, I., Lee, S., & Bui, D. T. (2020). Novel ensemble of multivariate adaptive regression spline with spatial logistic regression and boosted regression tree for gully erosion susceptibility. *Remote Sensing*, *12*(20), 3284. https://doi.org/10.3390/rs12203284

Rutebuka, J., De Taeye, S., Kagabo, D., & Verdoodt, A. (2020). Calibration and validation of rainfall erosivity estimators for application in Rwanda. *Catena*, *190,* 104538. https://doi.org/10.1016/j.catena.2020.104538

Santos, A. dos S., Silva Júnior, J. F. da, Santos, L. da S., Alencar Sobrinho, R. J., Amorim, E. C., Fernandes, G. S. T., Silva, E. F. da, Silva, T. G. F. da, de Lima, J. L. M. P., & Jardim, A. M. da R. F. (2025). Identification of priority areas for the control of soil erosion and the influence of terrain factors using RUSLE and GIS in the Caeté river casin, Brazilian Amazon. *Earth*, *6*(2), 35. https://doi.org/10.3390/earth6020035

Singh, M. C., Sur, K., Al-Ansari, N., Arya, P. K., Verma, V. K., & Malik, A. (2023). GIS integrated RUSLE model-based soil loss estimation and watershed prioritization for land and water conservation aspects. *Frontiers in Environmental Science*, *11,* 1136243. https://doi.org/10.3389/fenvs.2023.1136243

Sodoke, S., Andam-Akorful, S. A., Yahans Amuah, E. E., Amoah, E. G., Anokye, K., Nang, D. B., & Kazapoe, R. W. (2025). GIS-based assessment of soil erosion impact and mitigation strategies for sustainable agriculture in Ghana's most vulnerable region. *Environmental and Sustainability Indicators*, *25,* 100551. https://doi.org/10.1016/j.indic.2024.100551

Sun, C., Hou, H., & Chen, W. (2021). Effects of vegetation cover and slope on soil erosion in the Eastern Chinese Loess Plateau under different rainfall regimes. *PeerJ*, *9,* 11226. https://doi.org/10.7717/peerj.11226

Tarboton, D. G. (1997). A new method for the determination of flow directions and upslope areas in grid digital elevation models. *Water Resources Research*, *33*(2), 309–319. https://doi.org/10.1029/96WR03137

Terán-Gómez, V. F., Buitrago-Ramírez, A. M., Echeverri-Sánchez, A. F., Figueroa-Casas, A., & Benavides-Bolaños, J. A. (2025). Integrating AHP and GIS for sustainable surface water planning: Identifying vulnerability to agricultural diffuse pollution in the Guachal river watershed. *Sustainability*, *17*(9), 4130. https://doi.org/10.3390/su17094130

Thomas, I. A., Jordan, P., Mellander, P. E., Fenton, O., Shine, O., Ó hUallacháin, D., Creamer, R., McDonald, N. T., Dunlop, P., & Murphy, P. N. C. (2016). Improving the identification of hydrologically sensitive areas using LiDAR DEMs for the delineation and mitigation of critical source areas of diffuse pollution. *Science of the Total Environment*, *556*, 276–290. https://doi.org/10.1016/j.scitotenv.2016.02.183

Thomas, I. A., Jordan, P., Shine, O., Fenton, O., Mellander, P. E., Dunlop, P., & Murphy, P. N. C. (2017). Defining optimal DEM resolutions and point densities for modelling hydrologically sensitive areas in agricultural catchments dominated by microtopography. *International Journal of Applied Earth Observation and Geoinformation*, *54*, 38–52. https://doi.org/10.1016/j.jag.2016.08.012

Wischmeier, W. H., & Smith, D. D. (1978). *Predicting rainfall erosion losses. A guide to conservation planning* (No. 537.). U.S. Department of Agriculture, Science and Education Administration.

Yang, M., Yang, Q., Zhang, K., Pang, G., & Huang, C. (2024). Global soil erodibility factor (K) mapping and algorithm applicability analysis. *Catena*, *239,* 107943. https://doi.org/10.1016/j.catena.2024.107943

Zhang, K., Yu, Y., Dong, J., Yang, Q., & Xu, X. (2019). Adapting & testing use of USLE K factor for agricultural soils in China. *Agriculture, Ecosystems and Environment*, *269*, 148–155. https://doi.org/10.1016/j.agee.2018.09.033